Fatigue behavior of pultruded fiberglass tubes under tension, compression and torsion

Oleg Staroverov, Artur Mugatarov, Anastasia Sivtseva, Elena Strungar, Valeriy Wildemann
Center of Experimental Mechanics, Perm National Research Polytechnic University, Russia
cem_staroverov@mail.ru, oastaroverov@pstu.ru, https://orcid.org/0000-0001-6095-0962
cem_mugatarov@mail.ru, https://orcid.org/0000-0002-2229-8181
cem_sivtseva@mail.ru, https://orcid.org/0000-0002-4348-7491
cem.spaskova@mail.ru, https://orcid.org/0000-0002-2246-8638
wildemann@pstu.ru, https://orcid.org/0000-0002-6240-4022

Aleksandr Elkin, Ivan Sergeichev
Center for Materials Technologies, Skolkovo Institute of Science and Technology, Russia
aleksandr.elkin@skoltech.ru, https://orcid.org/0000-0003-2157-3425
i.sergeichev@skoltech.ru, https://orcid.org/0000-0002-4106-4372

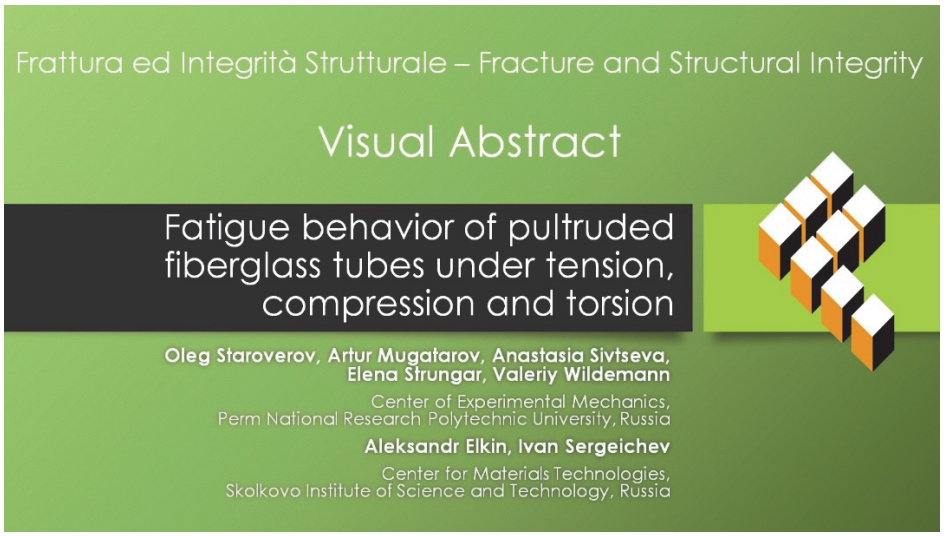

Citation: Staroverov, O., Mugatarov, A., Sivtseva, A., Strungar, E., Wildemann, V., Elkin, A., Sergeichev, I., Fatigue behavior of pultruded fiberglass tubes under tension, compression and torsion, Frattura ed Integrità Strutturale, 69 (2024) 115-128.

Received: 26.03.2024
Accepted: 25.04.2024
Published: 27.04.2024
Issue: 07.2024

KEYWORDS. Polymer composite, Pultruded fiberglass tubes, Fatigue, Damage accumulation, Stiffness degradation, Digital image correlation.

INTRODUCTION

Polymer composites replace conventional materials like metals in various industries (civil engineering, aerospace, marine, construction, etc.) due to such advantages as high corrosion resistance, lower weight and high mechanical characteristics [1–4]. Modern manufacturing technologies of glass fiber reinforced plastics (GFRP) allow to apply

them in structures subjected to heavy loads. One of the most popular production methods of composite structures is pultrusion [5–7], which is confirmed by the increasing application of pultruded GFRP. However, the number of works studying pultruded composites' mechanical properties is small compared to the number of studies devoted to composites produced by other methods. Accordingly, it is relevant to study the mechanical properties of pultruded composites.

Most composite structures are subjected to cyclic loads, causing fatigue and damages that decrease service life. Fatigue leads to a decrease in stiffness and strength of polymer composites [8–12]. Researchers distinguish two different degradation behaviors [13–18]. The first one is characterized by a slow decline of material stiffness, with a rapid transition to a significant decrease in stiffness, leading to fracture. The second behavior has three characteristic stages: initiation, described as a sharp decline in stiffness about 15-25% without a failure; stabilization, characterized by prolonged slow accumulation of fatigue damage; the final stage is aggravation, characterized by an intense decrease in stiffness, leading to the failure. However, the stiffness degradation processes of pultruded GFRP were not thoroughly studied [19–23]. Hence, it is necessary to investigate fatigue behavior and damage accumulation of pultruded composites. Moreover, since composites have anisotropic nature, it is necessary to take it into account and study fatigue under different loading modes (i.e., tensile, torsion, bending, etc.).

Various models of fatigue damage accumulation processes' descriptions were proposed [24–29]. Earlier the models of residual dynamic stiffness' dependence on number of loading cycles were developed by Yang et al. [30], Whitworth [31], Mao and Mahadevan [32], Van Paepegem and Degrieck [33], Wu and Yao [34], Shiri et al. [35], Zong and Yao [36], Wang and Zhang [37], Gao et al. [38–40], etc. The authors of this work previously developed and successfully applied the composites' properties degradation models based on cumulative distribution functions (Weibull distribution, beta distribution) [41, 42]. Besides, the method for calculating damage accumulation stage boundaries was proposed using the characteristic value of mechanical property decrease rate [15].

This work is devoted to an experimental investigation of fatigue behavior of pultruded fiberglass tubes under uniaxial tension, compression and torsion. The section "Material and methods" describes the composite material, testing procedures, specimen preparation and equipment. In the subsection "Static tests results" the results of the composite's tensile, compression, and torsion tests are provided, and the static mechanical properties and failure mechanisms are described. In the "Fatigue test results" subsection, the fatigue curves are presented for tension-tension, tension-compression, compression-compression, and torque (shear) modes. The main damage mechanisms are described. In the subsection "Stiffness degradation analysis", the material's dynamic stiffness reduction is shown, and the data is processed with the previously developed model. The dependence of model parameters on the loading conditions is determined. The section "Conclusions" summarizes the work's main outcome and provides an outlook for further research.

MATERIAL AND METHODS

Material and specimens' preparation

The material is pultruded fiberglass (JSC "FloTenk", Russia) manufactured in accordance with GOST 33344–2015 (which corresponds to EN 13706-1:2003, EN 13706-2:2003, EN 13706-3:2002). The typical scheme of the pultrusion process is shown in the Figure 1a [21]. The composite has a three-layer structure. The outer layers are chaotically oriented continuous fiber glass mat Unifilo U528 with a thickness of 0.4–0.7 mm. The inner layer (roving) consists of unidirectional glass fibers of diameter 24 um and linear density 4800 tex. Aropol S 560 ZX polyester unsaturated resin is used as a matrix. The mass content of resin is 36%, mat 26% and roving 36%. During the pultrusion process a transition zone was formed in which mat layers intersect the roving. Figure 1b shows the microstructure of the composite. The tubes were cut into 140 mm long pieces to fabricate the specimens. Previous studies indicated [43] that the optimal way to fix the specimens in the grips of the testing system is to use aluminum cylindrical tabs, which are glued into the specimen ends. The gauge length was approximately 60 mm, the grip (tab) length was 40 mm, outer diameter ≈32 mm, inner diameter was equal to 26 mm. An example of the prepared specimen is shown in Figure 1c.

Equipment

Experimental studies were carried out using the large-scale research facilities "Complex of testing and diagnostic equipment for studying properties of structural and functional materials under complex thermomechanical loading" at the Center of Experimental Mechanics of the Perm National Research Polytechnic University (PNRPU).

The uniaxial static and fatigue tests were conducted using a two-axis servohydraulic system Instron 8802 (United Kingdom) with the following characteristics: maximum tension/compression load is ±100 kN, maximum torque is 1000 N·m, accuracy is 0.5% of the measured value, loading frequency is up to 30 Hz. The unit includes a FastTrack controller with WaveMatrix software support. A built-in feedback module allows to adjust the applied force as the specimen stiffness changes to maintain

the specified loading conditions. A non-contact optical video system VIC-3D with Prosilica GE4900 cameras with a resolution of 4872 x 3248 (16 megapixels) and a maximum acquisition rate of 3 frames/second was used to determine the displacements on the surface of fiberglass tubular specimens. The digital image correlation (DIC) method implemented in the VIC-3D software was used to calculate strain fields.

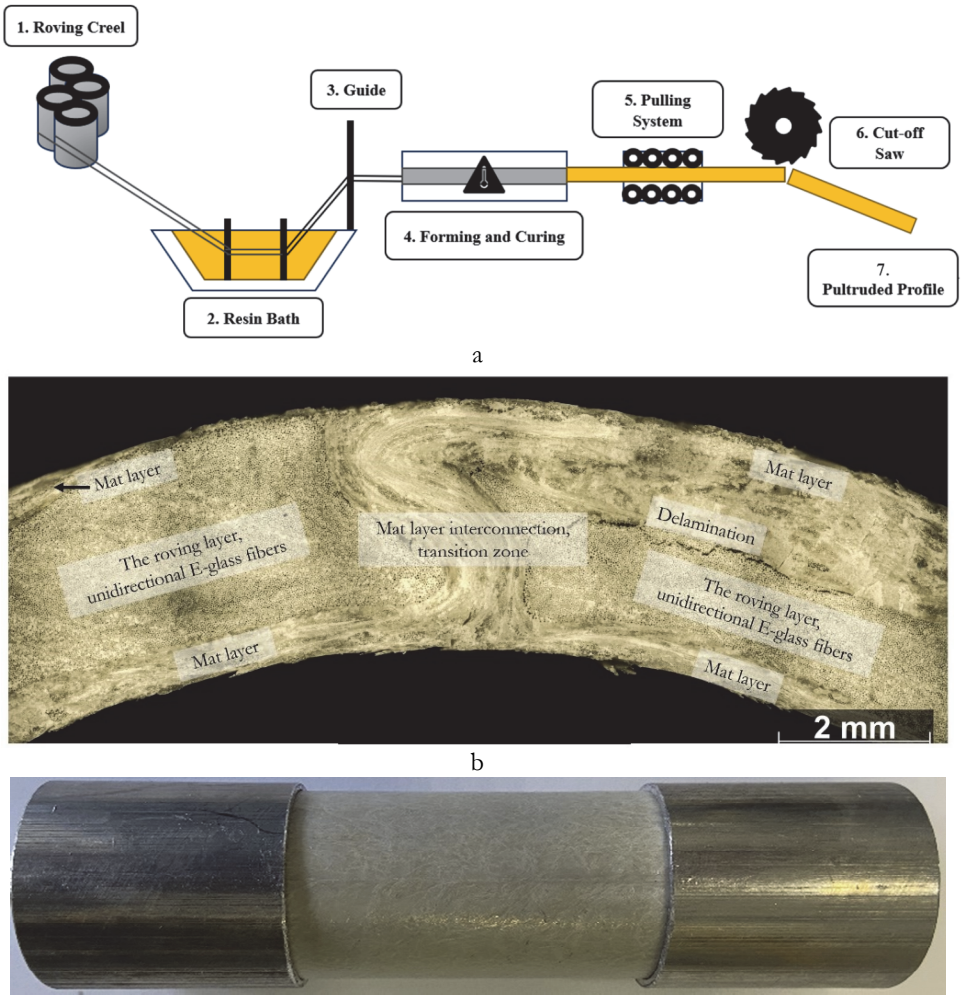

Figure 1: Typical scheme of the pultrusion process [21] (a), structure of the pultruded fiberglass tube (b) and image of the prepared specimen (c).

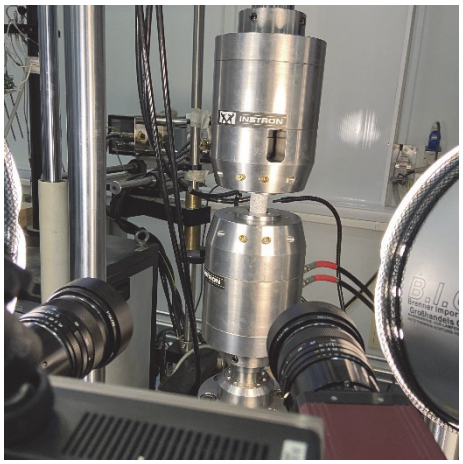

Figure 2: Specimen in the Instron 8802 grips and VIC-3D.

Methods

The static tests were performed in tension, compression, and torsion to determine the tensile, compressive and shear strength, as well as the elastic moduli. The displacement rate was 2 mm/min for tensile and compressive tests (according to the recommendations of ASTM D3039 and ASTM D3410), while the twisting rate was 20 deg/min for torsion tests. Stress-strain curves were obtained using the VIC-3D. The evolution of strain fields on the surface of the specimens was investigated. The obtained ultimate stress values were used to determine the parameters for further fatigue tests.

The axial fatigue tests were conducted in tension-tension, compression-compression, tension-compression modes in accordance with the recommendations of ASTM D3479. The torsional fatigue tests were conducted with a symmetric cycle. The magnitude of the load was chosen to have the maximum number of fatigue cycles approximately $N = 5 \cdot 10^5$. A sinusoidal loading cycle was applied, the loading schemes, stress ratio (R) and frequency (ν) values are given in Table 1. The maximum stress amplitude was in range of 30–95% of the ultimate strength to break specimens at approximately 10^2, 10^3, 10^4 and 10^5 fatigue cycles. The fatigue S-N curves were approximated by the Basquin relationship [44].

Fatigue loading mode	Loading scheme	Stress ratio (R)	Frequency (ν), Hz
Tension-tension	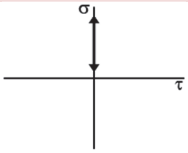	0.1	4
Compression-compression	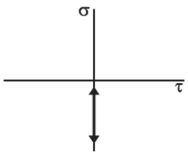	10	4
Tension-compression	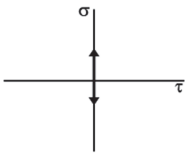	–0.78 ($\approx -\sigma_{B\_comp}/\sigma_{B\_tens}$)	2
Torsion	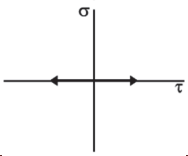	–1	2

Table 1: Loading conditions of fatigue tests.

Stiffness degradation data and its analysis

To investigate the degradation of the dynamic stiffness, the amplitudes of axial load, axial displacement, torque and twist angle were recorded every 1st, 10th, 100th fatigue cycle. Moreover, these values were recorded for each of the last hundred fatigue cycles for specimens subjected to the high load amplitude. Dynamic tensile/compression stiffness was defined as the ratio of axial load amplitude to axial displacement amplitude. Dynamic torsional stiffness was defined as the ratio of torque amplitude to twist angle amplitude. Since the geometry has a certain variability, normalized values of residual dynamic stiffness were used for comparison. The K_{SE} represents the ratio of the current dynamic stiffness to that obtained at the tenth cycle for tension/compression fatigue tests. The first values of dynamic stiffness were discarded because of high stiffness of the specimens in the axial direction. The label K_{SG} is the ratio of the current dynamic torsional stiffness to the one obtained at the first cycle. Since the decrease of stiffness is dramatic in the last fatigue cycles, a drop in dynamic stiffness to a value of 0.75 for tension/compression and 0.3 for torsion was considered.

The data on residual stiffness were presented in the form of function $K_S(n)$, where $K_S = K_{SE}$ or K_{SG} and $n = N/N_0$ – a fatigue cycle ratio, N – number of a current cycle, N_0 – number of fatigue cycles for a certain specimen. To analyze the decrease of dynamic stiffness, the earlier proposed model based on the use of the Weibull cumulative probability distribution function was utilized [41]:

$$K_S = 1 - \lambda\left(-\ln\left(1-n\right)\right)^{\frac{1}{\kappa}}. \quad (1)$$

Here, λ and κ are the non-negative fitting parameters. The stages of damage accumulation and damage rates are determined using the derivative of the damage function $\omega_S = 1–K_S$:

$$\omega_S' = \frac{\lambda}{\kappa}\left(-\ln\left(1-n\right)\right)^{\frac{1}{\kappa}-1}\frac{1}{1-n}. \tag{2}$$

If $\kappa < 1$ the function $\omega'_S(n)$ is monotonically increasing, which provides the realization of two-stage diagram of stiffness degradation (i.e., the stage of slow stiffness decrease is realized, which is replaced by the stage of fast stiffness decrease). However, if $\kappa \geq 1$ the function is undefined for $n = 0$, and a three-stage diagram of dynamic stiffness degradation is realized (i.e., initiation, stabilization and aggravation stages are realized). Thus, we conclude that the proposed model is flexible enough to describe both types of damage accumulation regularities.

RESULTS AND DISCUSSION

Static tests results

The static test results in a form of strain-stress curves are presented in Figure 3. The ultimate tensile strength is σ_{B_tens} = 323.7±30.6 MPa, the ultimate compressive strength σ_{B_comp} = 251.4±23.5 MPa, the maximum shear strength is τ_B = 54.0±2.1 MPa. The results demonstrate that tensile and compressive behavior is linear-elastic, but the torsional behavior of the material is nonlinear. After the shear strength is reached, an extended stage of postcritical deformation was observed. The difference in behavior is related to the fact that in tension/compression, most of the load is carried by the roving, while in torsion, the load is carried mainly by the matrix and mat layers. Postcritical deformation of polymer composites was also noticed in the works [45–46]. This feature could be explained as pseudoplasticity resulting from the accumulation of structural damage [47–48].

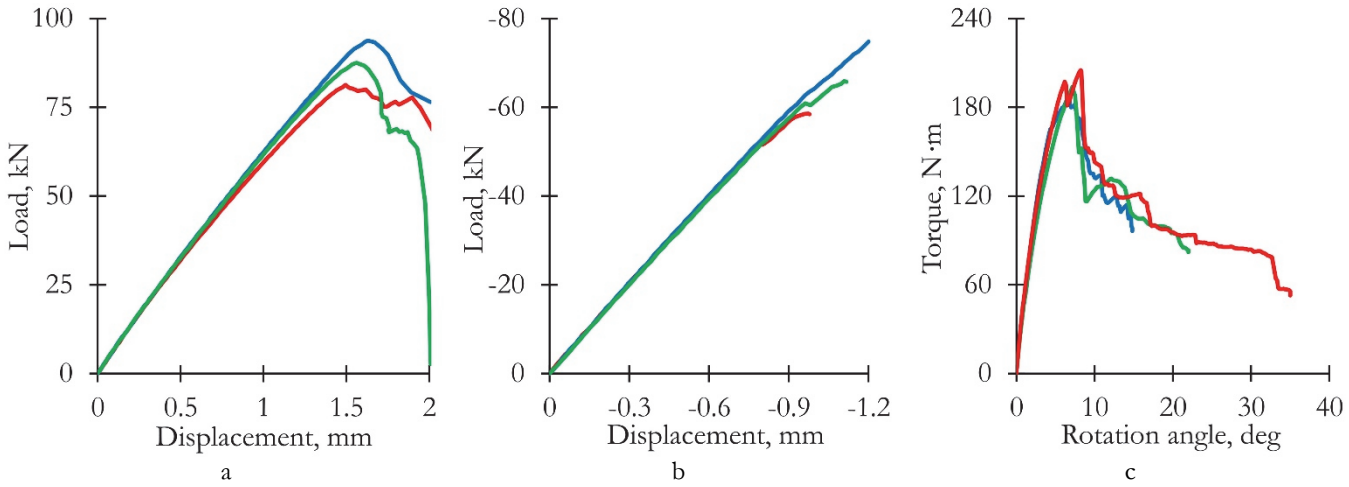

Figure 3: Typical loading diagrams of pultruded fiberglass tubes under static: tension (a), compression (b), torsion (c).

Using the VIC-3D and DIC method, the stress-strain curves were constructed for static tests under tension, compression and torsion (Figure 4). The average values of elastic moduli were determined: in tension/compression Young's modulus was equal to ≈30 GPa, in torsion shear modulus was equal to ≈3 GPa. The analysis of strain fields evolution demonstrated that primary localizations occurred in the shape of separate spots at 50% of the maximum tensile load. These localizations are formed due to chaotic stacking of glass fibers on the surface of mat layer. The difference between the maximum and minimum strain values is higher at increased loads. The longitudinal strains at the maximum load clearly demonstrate the defect zone that leads to failure of the specimen. In comparison, no zones of localized strains were observed under compression. It indicates that the deformation process of the material is more homogeneous under compressive loading, which might be explained by the predominant work of the matrix rather than fibers. Under the torsion, the localization of shear strains was formed in the shape of spots. At the maximum torque value, the zone of localized shear corresponded to the place, where the damage and cracks propagation occurred. The strain fields evolution is shown in Figure 4.

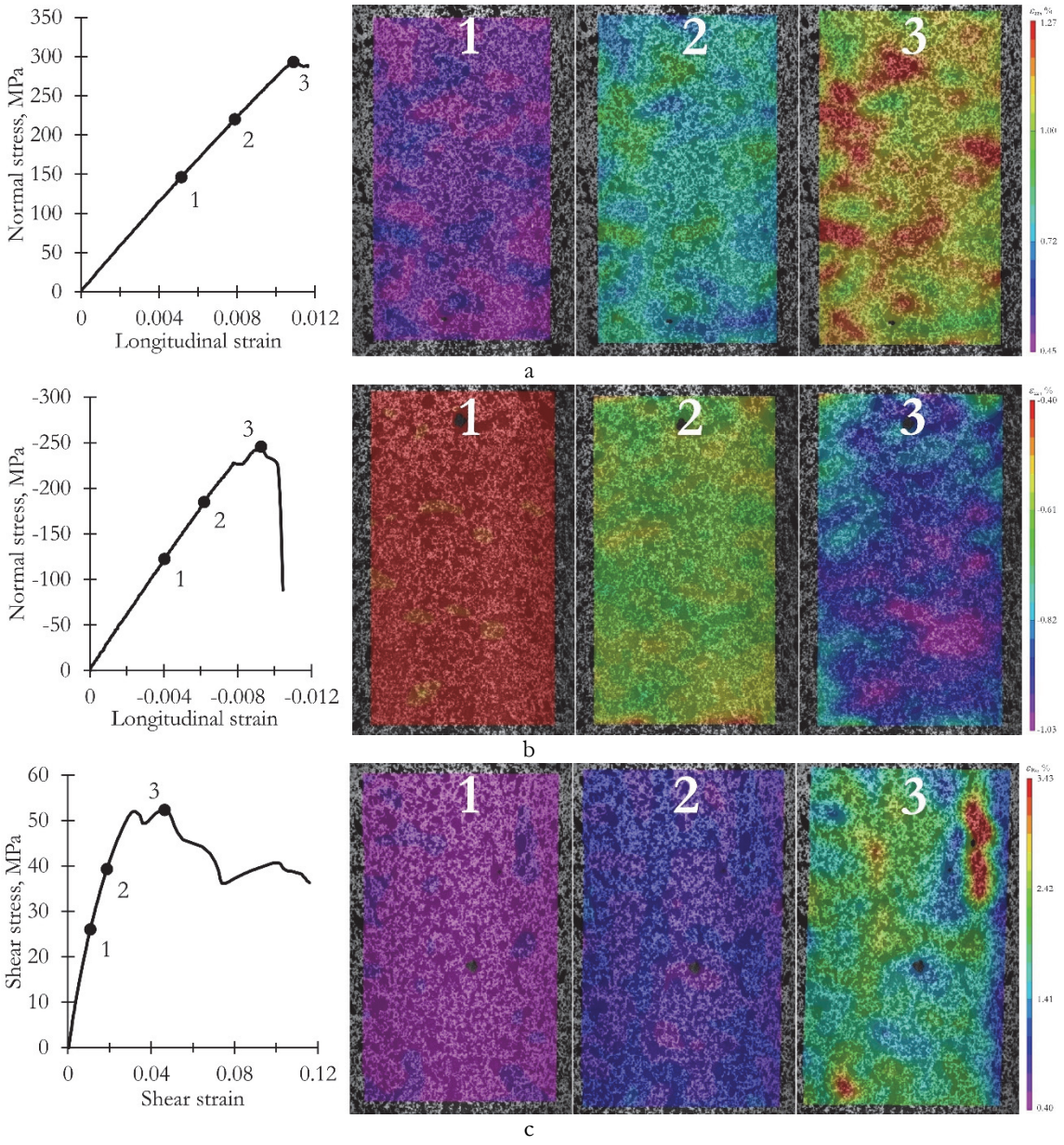

Figure 4: Strain fields evolution under static: tension (a), compression (b), torsion (c).

The analysis of the fractured surfaces was carried out (presented in Figure 5). The tensile fracture occurred in the middle of the specimen. The cracks of complex geometry initiated in the outer mat layer and propagate along the specimen and lead to delamination between the roving and mat layers. The crack was oriented along the specimen axis and along the transition zone with mat layer interconnection. Unidirectional fiber breaking occurred in the roving layer, leading to abrupt failure. Under compression, the fracture occurred near the grips, and the compressive failure was due to fiber breaking and local buckling in the roving layer and debonding of mat layers. Under torsion, fracture occurred both in the gauge area and near the grips. The surface cracks in the outer mat layer indicated delamination from the roving. The roving had a matrix failure which led to loss of stability of the specimen under torsion.

Fatigue tests results

The maximum stress amplitudes were defined based on the static test results. The tension-tension fatigue tests with a stress ratio $R = 0.1$ were conducted at a maximum stress amplitude corresponding to 0.38–0.89 of the ultimate tensile strength. The compression-compression fatigue tests with $R = 10$ were performed with an amplitude of 0.49-0.92 of the ultimate compressive strength. The tension-compression fatigue tests with $R = -0.78 \approx -\sigma_{B\_comp}/\sigma_{B\_tens}$ were conducted at a maximum

tensile stress amplitude of 0.30–0.73 of the ultimate tensile strength. The torsional fatigue tests were done with $R = -1$ at a maximum tangential stress equal to 0.30–0.54 of the ultimate shear strength. The fatigue data was approximated by the Basquin relationship:

$$\sigma_{\max} = \sigma_f N_0^{\ b}, \ \tau_{\max} = \tau_f N_0^{\ b}. \tag{3}$$

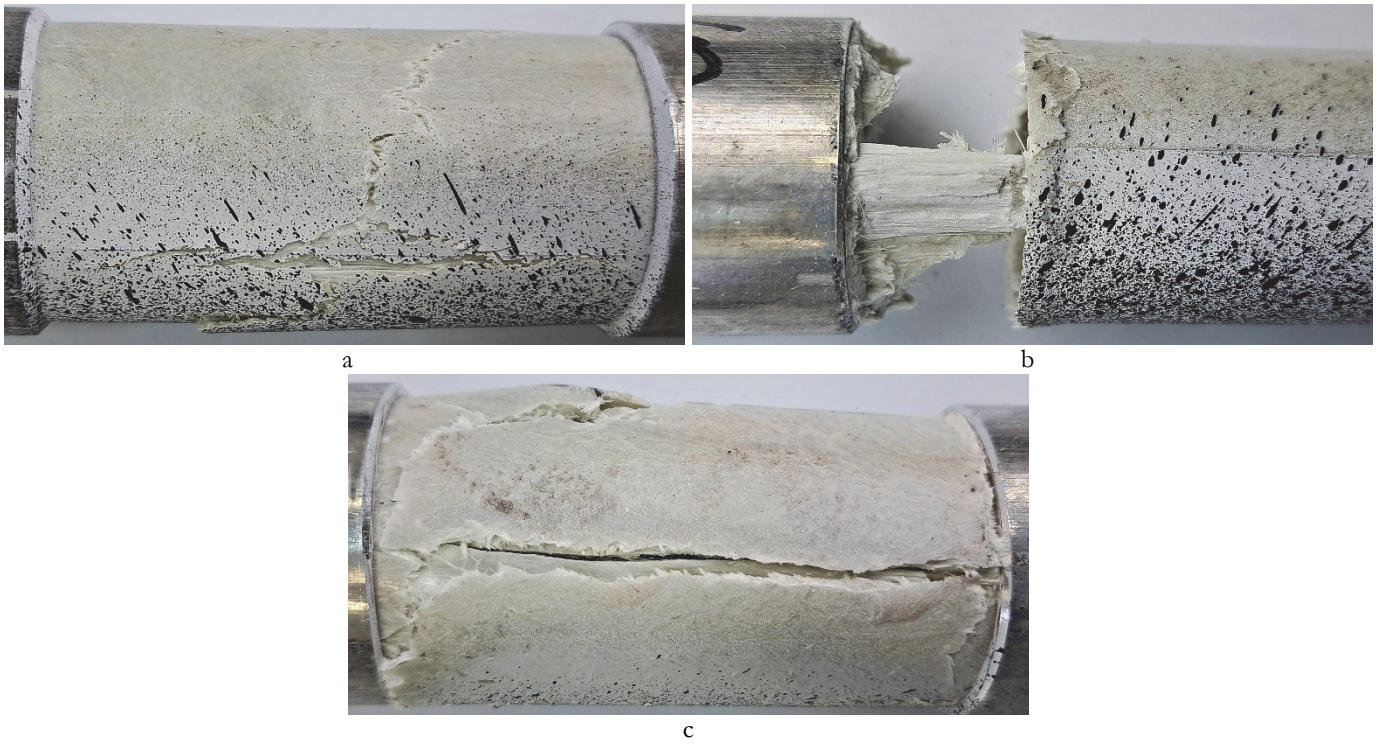

a b c

Figure 5: Images of specimens after static: tension (a), compression (b), torsion (c).

Coefficients σ_f, τ_f, b are the fitting coefficients. The approximated S-N curves, Basquin parameters, coefficients of determination R^2, and raw fatigue data are presented in Figure 6.

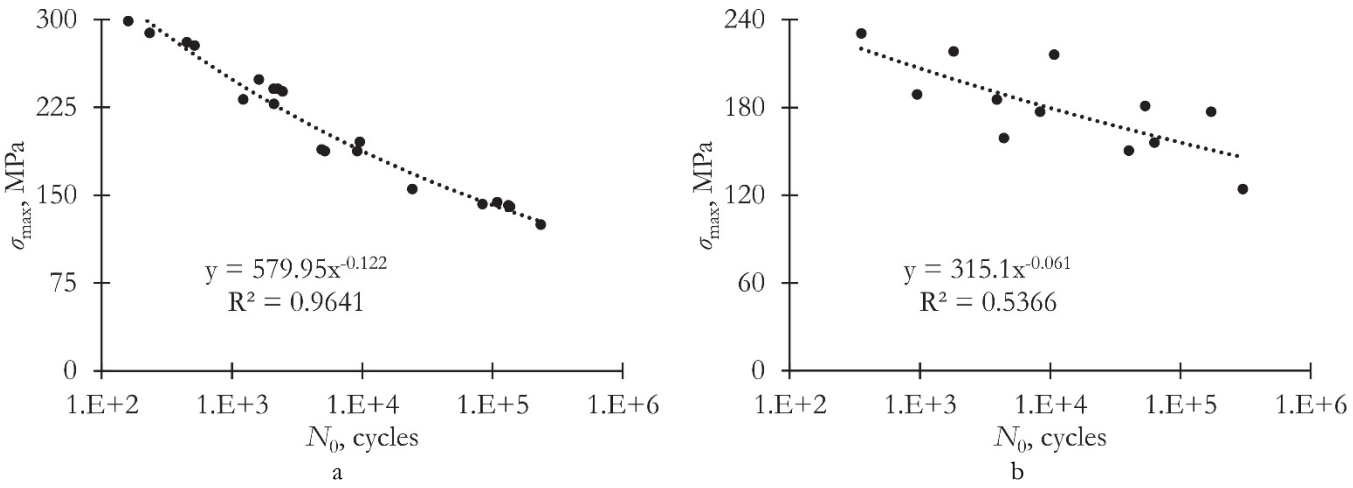

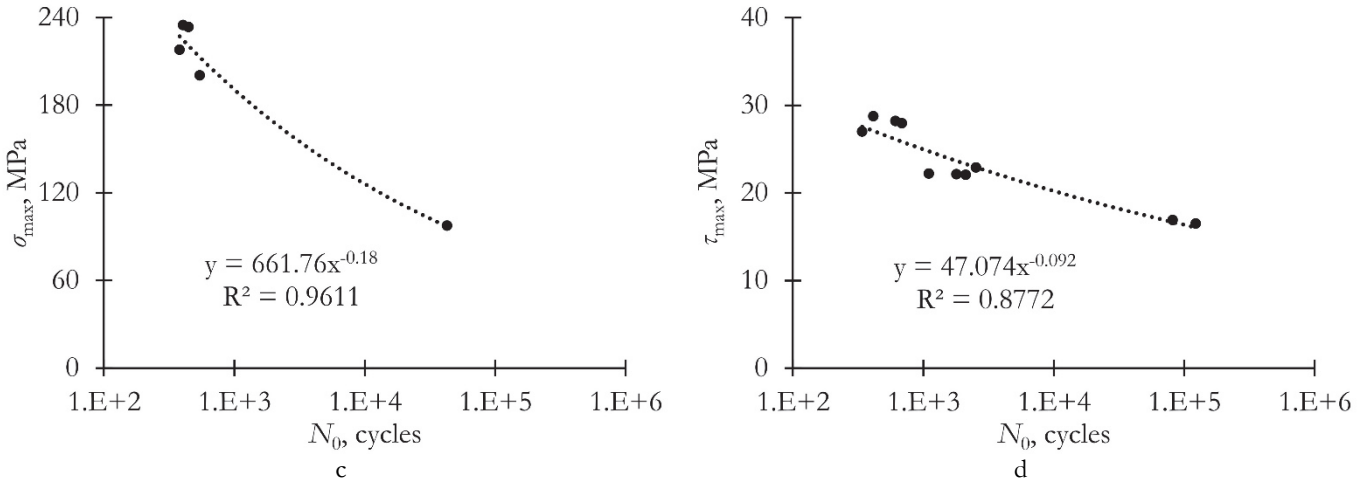

Figure 6: Fatigue curves of pultruded fiberglass tubes under cyclic: tension-tension (a); compression-compression (b); tension-compression (c); torsion (d).

Fracture analysis of pultruded GFRP specimens after fatigue tests was carried out (Figure 7). After tension-tension mode, fracture of the roving layer occurred near the gripping part, while the mat layer debonded from the roving and cracked. The presence of more than one crack on the surface of the specimens was observed. After compression-compression fatigue, the specimen had a similar to static compression failure, describing by fiber buckling and fracture. However, the fatigue fracture has a more complex shape and passes not only near the grip, but also along the middle of the specimens. After tension-compression fatigue, a mixed damage mechanism was observed: there are fiber buckling near the grips and fractured fibers with mat delamination in the middle of the specimen. After torsion fatigue tests multiple cracking processes are observed on the mat layer surface, but crack propagation was in the roving layer as well. The loss of stability during torsion fatigue was not observed, which was associated with a small amplitude of applied shear stresses.

Figure 7: Images of specimens after cyclic: tension-tension (a); compression-compression (b); tension-compression (c); torsion (d).

Stiffness degradation analysis

The data of dynamic stiffness over fatigue cycles were approximated by function $K_S(n)$, see eq.1; the resultant curves for $K_S(n)$ and $\omega'_S(n)$ are shown in Figure 8 (the stiffness degradation curves are presented on the left and damage growth rate

on the right). Dots on the graphs indicate experimental data, solid lines - their approximation by the model. Green graphs represent the results for low ratio between maximum stress in the cycle and ultimate strength, red graphs - for high ratio. As described in the work [42], the following damage growth rate was accepted at which the fatigue damage accumulation stages change: $\delta = 0.3$ stiffness change along the longitudinal (fiber) axis, $\delta = 0.5$ stiffness change under torsion (represented as black dotted lines in Figure 8). Vertical dashed lines in Figure 8 represent a boundary line separating various stages of damage accumulation. The coefficient of determination was the following range: $R^2 = 0.86–0.99$ for tension-tension mode; $R^2 = 0.70–0.99$ for compression-compression; $R^2 = 0.83–0.99$ for tension-compression; $R^2 = 0.93–0.99$ to torsion. Two-stage damage accumulation behavior was indicated for all axial modes, meanwhile the parameter λ is relatively low. The duration of the first low damage accumulation (low stiffness loss) stage is 80–95% of the total fatigue life. An increase in the maximum stress amplitude does not significantly change the type of stiffness degradation curves. In the compression-compression mode, a similar two-stage damage accumulation behavior was observed. However, a three-stage diagram of stiffness degradation was realized in half of the cases, but the duration of the initiation stage was concise. In torsion, a distinguished three-stage pattern of stiffness degradation is observed. The duration of the stabilization stage is about 50% of the total fatigue life and it this stage starts at 20% of fatigue life. The variation of the maximum stress amplitude affects the damage accumulation (i.e., stiffness loss). These might be explained as follows: load along the fiber axis is carried mainly by fibers and a few of their ruptures occur (i.e. the properties decrease only slightly), while the shear load is carried by the matrix, in which intensive cracking processes can occur, leading to a steady and significant loss in torsional stiffness.

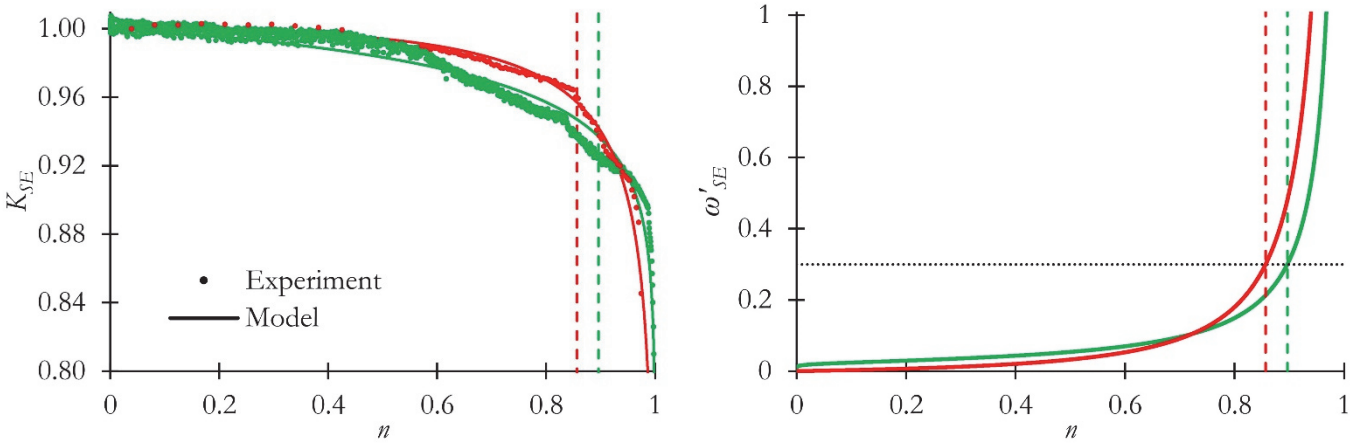

a

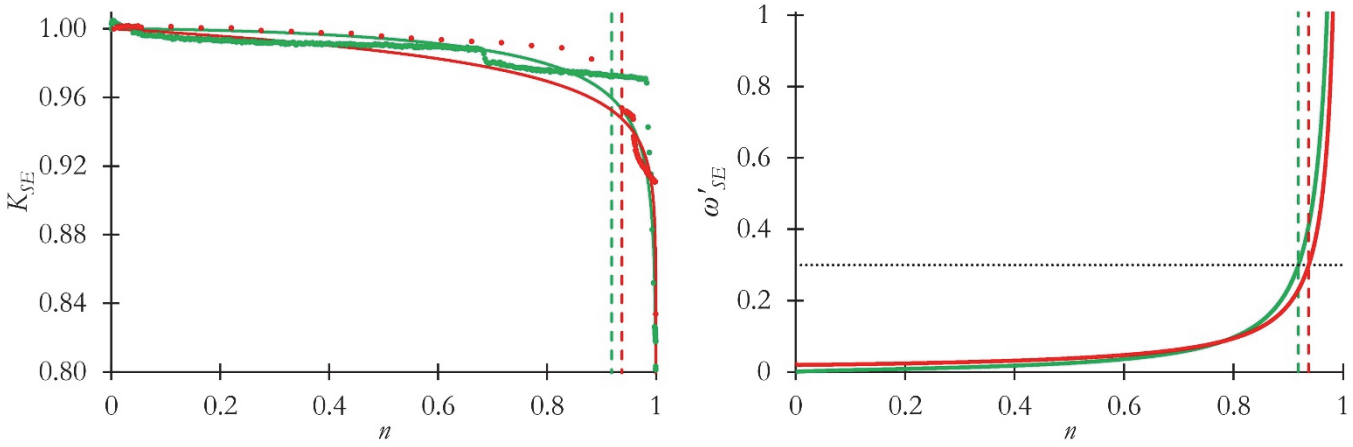

b

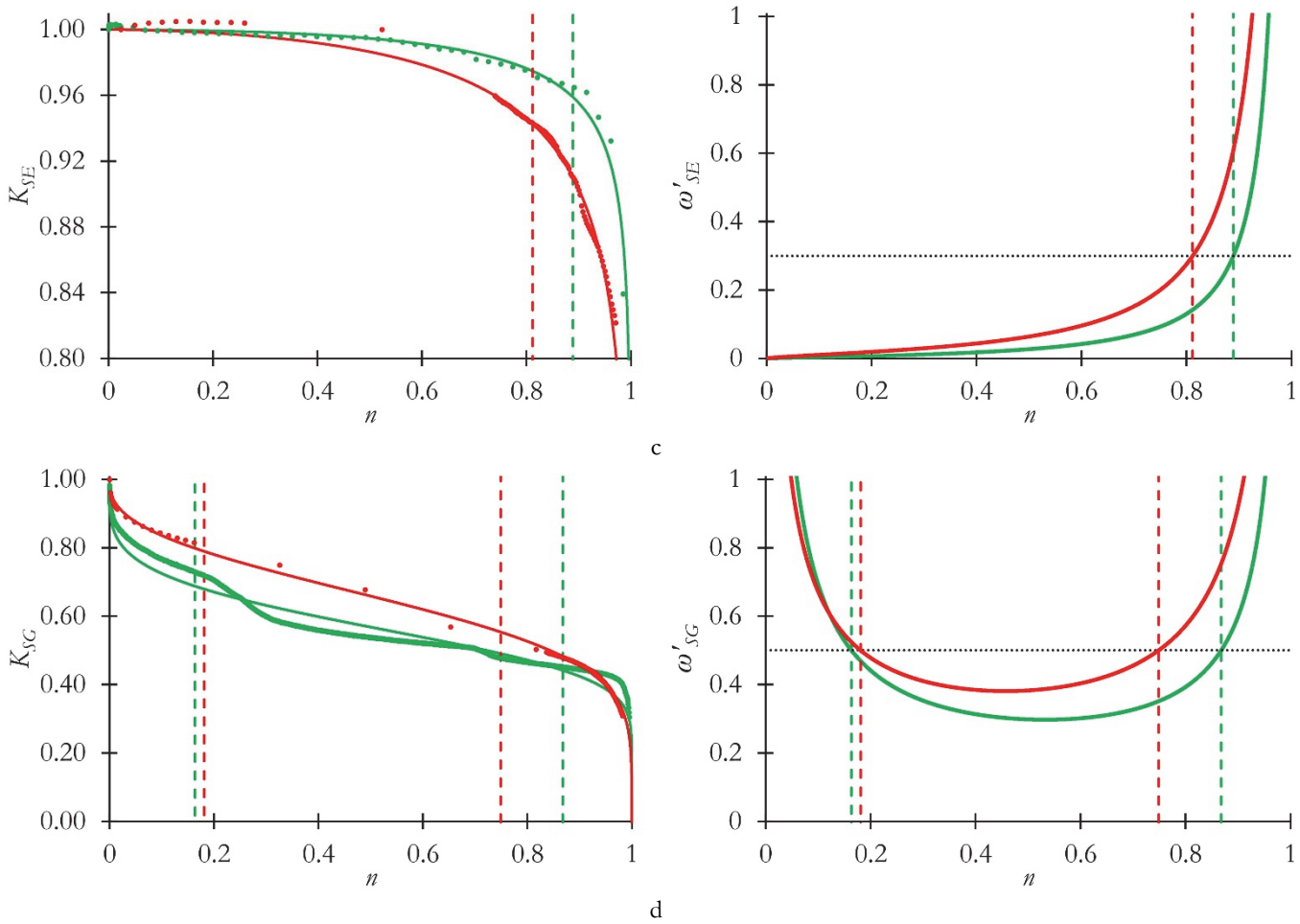

Figure 8: Typical stiffness degradation and damage parameter growth rate curves (on the left and right respectively) for specimens during cyclic: tension-tension (a); compression-compression (b); tension-compression (c); torsion (d). Green curves are built for the specimens with a low ratio between the maximum stress during the cycle and ultimate strength, red lines are built for the specimens with the high one. Dotted curves are experimental data; solid lines are the data fitting by the proposed model; dashed lines represent damage accumulation stages' boundaries; black dotted lines on the right side show the critical value of damage parameter derivative.

To evaluate the influence of the maximum stress amplitude on damage accumulation, the Pearson correlation coefficient (PCC, denoted as r) was calculated. The results are presented in Figure 9. It was found that the model parameters κ и λ for tension-tension, compression-compression and tension-compression modes are practically independent from stress amplitude at a certain stress ratio R. Average value of the parameters: $\kappa = 0.6347$ and $\lambda = 0.0204$ for tension-tension mode with $R = 0.1$; $\kappa = 1.5422$ and $\lambda = 0.0267$ for compression-compression ($R = 10$); $\kappa = 0.5410$ and $\lambda = 0.0118$ for tension-compression mode ($R = –0.78$). Thus, we conclude that the model parameters depend weakly on the stress amplitude, while their values change significantly when the mean normal stress value changes (a transition from a two-stage to a three-stage diagram was observed when moving into the compression region). In opposite, the analysis of torsion fatigue tests indicated significant correlation between the maximum stress amplitude and the model parameters. The dependencies were approximated by a linear function for the parameter λ and a quadratic function for the parameter κ (Figure 9d).

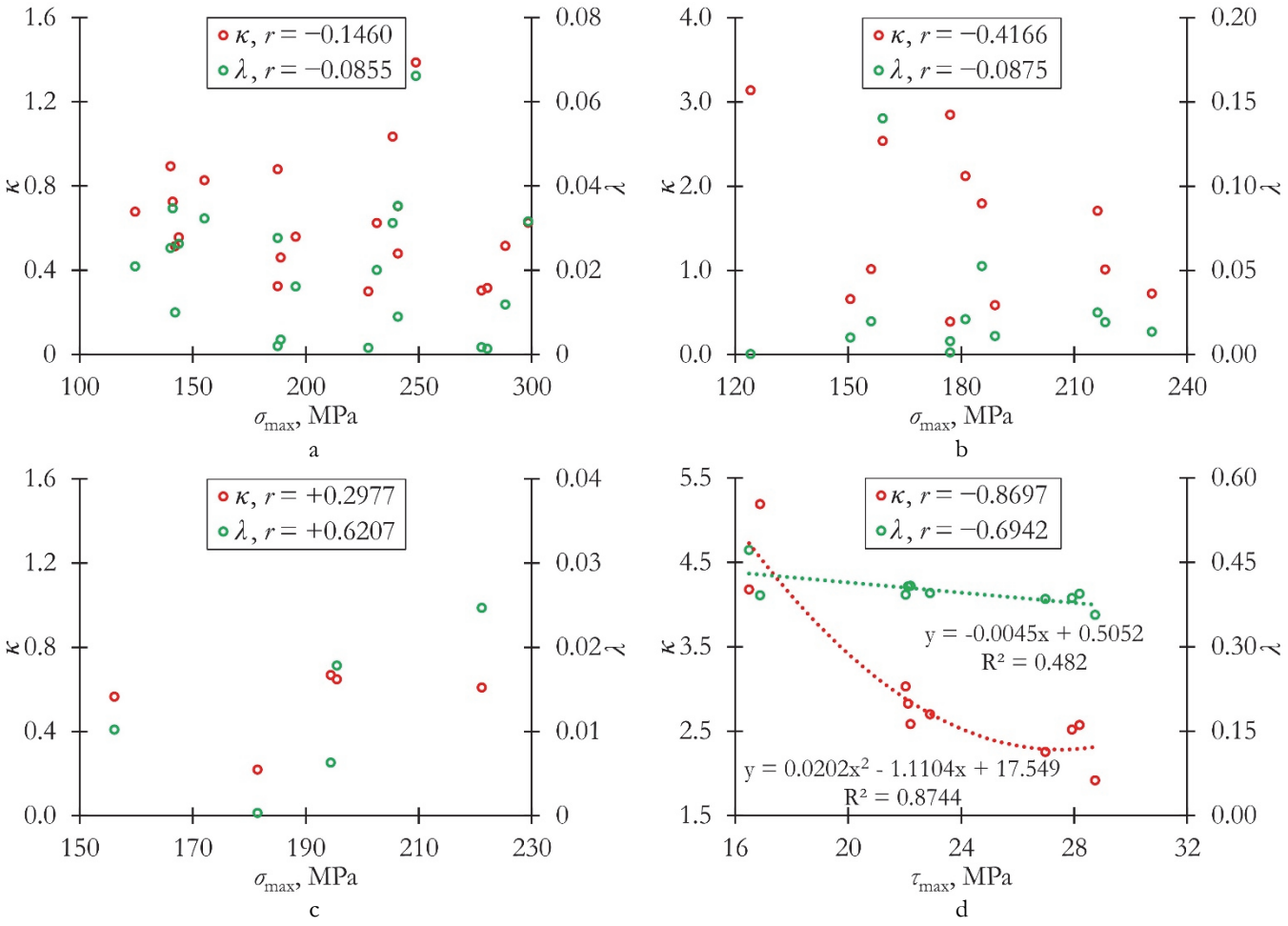

Figure 9: Model parameters dependence on maximum stress value for various loading modes: tension-tension (a); compression-compression (b); tension-compression (c); torsion (d).

Conclusions

This work experimentally investigated the fatigue behavior of pultruded fiberglass tubes under uniaxial tension, compression, and torsion. The main outcomes of the study are the following:

1. The static mechanical properties of the pultruded GFRP tubes under tension, compression and torsion were obtained. The localizations of the strains have been studied using the DIC method. The postcritical deformation stage has been found out under torsion loading.

2. The fatigue S-N curves have been built under cyclic tension-tension, compression-compression, tension-compression and torsion modes using the Basquin equation.

3. Typical damaging mechanisms have been described. Fibers breakage in the roving and crack propagation in the mat layer occurred under tensile loads; fiber crushing near the grips was observed only under compression; multiple cracks in the mat and roving resulted resulting loss of specimen stability under torsion.

4. The stiffness degradation model demonstrated high descriptive capability. It describes the two-stage and three-stage damage accumulation that correspond to axial and torsional loading, respectively.

5. The correlation analysis between the model parameters (κ and λ) and the maximum stress amplitude demonstrated a significant correlation only under torsion. The maximum stress amplitude does not influence stiffness degradation behavior under axial loadings.

Experimental results showed significantly different axial and torsional fatigue behavior of pultruded GFRP. The further research should be devoted to the investigation of the multiaxial fatigue behavior.

ACKNOWLEDGEMENTS

The work was carried out with support of the Russian Science Foundation (Project № 22-79-00136, https://rscf.ru/project/22-79-00136/) in the Perm National Research Polytechnic University.

REFERENCES

[1] Qureshi, J. (2022). A Review of fibre reinforced polymer structures, Fibers, 10(27). DOI: 10.3390/fib10030027.
[2] Rajak, D. K., Wagh, P. H., Kumar, A., Behera, A., Pruncu, C. I. (2022). Advanced polymers in aircraft structures, In: Materials, Structures and Manufacturing for Aircraft, Cham, Springer, pp. 65–88. DOI: 10.1007/978-3-030-91873-6_3
[3] Rubino, F., Nistico, A., Tucci, F., Carlone, P. (2020). Marine application of fiber reinforced composites: a review, J. Mar. Sci. Eng., 8(1), 26. DOI: 10.3390/jmse8010026.
[4] Ali, H. T., Akrami, R., Fotouhi, S., Bodaghi, M., Saeedifar, M., Yusuf, M., Fotouhi, M. (2021). Fiber reinforced polymer composites in bridge industry, Structures, 30, pp. 774–785. DOI: 10.1016/j.istruc.2020.12.092.
[5] Vedernikov, A. Safonov, A., Tucci, F., Carlone, P., Akhatov, I. (2020). Pultruded materials and structures: A review, J. Compos. Mat., 54(26), pp. 4081–4117. DOI: 10.1177/0021998320922894.
[6] Arrabiyeh, P. A., May, D., Eckrich, M., Dlugaj, A. M. (2021). An overview on current manufacturing technologies: Processing continuous rovings impregnated with thermoset resin, Polym. Compos., 42.(11), pp. 5630–5655. DOI: 10.1002/pc.26274.
[7] Mindermann, P., Witt, M. U., Gresser, G. T. (2022). Pultrusion-winding: A novel fabrication method for coreless wound fiber-reinforced thermoset composites with distinct cross-section, Compos. - A: Appl. Sci. Manuf., 154, 106763. DOI: 10.1016/j.compositesa.2021.106763.
[8] Lei, Z., Pan, R., Sun, W., Dong, Y., Wan, Y., Yin, B. (2024). Fatigue damage mechanisms and evolution of residual tensile strength in CFRP composites: Stacking sequence effect, Compos. Struct., 330, 117818. DOI: 10.1016/j.compstruct.2023.117818.
[9] Singh, K. K., Ansari, M .T. A., Azam, M. S. (2021). Fatigue life and damage evolution in woven GFRP angle ply laminates, Int. J. Fatigue, 142, 105964. DOI: 10.1016/j.ijfatigue.2020.105964.
[10] Roundi, W., El Mahi, A., El Gharad, A., Rebiere, J-L. (2019). Experimental investigation of the fatigue behavior of glass/epoxy composites evaluated by the stiffness degradation and damage accumulation, J. Compos. Mater., 53(6), pp. 731–740. DOI: 10.1177/0021998318790341.
[11] Elenchezhian, M. R. P., Das, P. P., Rahman, M., Vadlamudi, V., Raihan, R., Reifsnider, K. (2021). Stiffness degradation in fatigue life of composites using dielectric state variables, Compos. Struct., 273, 114272. DOI: 10.1016/j.compstruct.2021.114272.
[12] Chaves, M. C., Castro, D., Pertuz, A. (2024). Uniaxial fatigue study of a natural-based bio-composite material reinforced with fique natural fibers, Frattura ed Integrità Strutturale, 68, pp. 94–108 DOI: 10.3221/IGF-ESIS.68.06.
[13] Zangenberg, J., Brøndsted, P., Gillespie Jr, J. W. (2014). Fatigue damage propagation in unidirectional glass fibre reinforced composites made of a non-crimp fabric, J. Compos. Mater., 48(22), pp. 2711–2727. DOI: 10.1177/0021998313502062.
[14] D'Amore, A., Grassia, L. (2017). Phenomenological approach to the study of hierarchical damage mechanisms in composite materials subjected to fatigue loadings, Compos. Struct., 175, pp. 1–6. DOI: 10.1016/j.compstruct.2017.04.071.
[15] Wil'deman, V. E., Staroverov, O. A., Lobanov, D. S. (2018). Diagram and parameters of fatigue sensitivity for evaluating the residual strength of layered GFRP composites after preliminary cyclic loadings, Mech. Compos. Mater., 54, pp. 313–320. DOI: 10.1007/s11029-018-9741-9.
[16] Eliopoulos, E. N., Philippidis, T. P. (2011) A progressive damage simulation algorithm for GFRP composites under cyclic loading. Part I: Material constitutive model. Compos. Sci. Technol., 71(5), pp. 742–749. DOI: 10.1016/j.compscitech.2011.01.023.
[17] Bogdanov, A., Eremin, A., Burkov, M., Panin, S., Lyubutin, P. (2023). Estimating degradation of strength of neat PEEK and PEEK-CF laminates under cyclic loading by mechanical hysteresis loops, Frattura ed Integrità Strutturale, 66, pp. 152–163. DOI: 10.3221/IGF-ESIS.66.09.

[18] Elkin, A., Gaibel, V., Dzhurinskiy, D., Sergeichev, I. (2022). A multiaxial fatigue damage model based on constant life diagrams for polymer fiber-reinforced laminates, Polymers, 14(22), 4985. DOI: 10.3390/polym14224985.
[19] Tonatto, M. L. P., Tarpani, J. R., Amico, S. C. (2022). Short-beam shear fatigue behavior of round curved pultruded composite, Mech. Adv. Mater. Struct., 29(26), pp. 5579–5587. DOI: 10.1080/15376494.2021.1959968.
[20] Gao, Q., Xin, H., Zhang, Y. (2023). Experimental investigation on transverse tension-tension fatigue behavior of pultruded glass-fiber reinforced polymer (GFRP) unidirectional lamina, Constr. Build. Mater., 399, 132527. DOI: 10.1016/j.conbuildmat.2023.132527.
[21] Balakrishnan, T. S., Sultan, M. T. H., Shahar, F. S., Basri, A.A., Shah, A. U. M., Sebaey, T. A., Łukaszewicz, A., Józwik, J., Grzejda, R. (2024). Fatigue and impact properties of kenaf/glass-reinforced hybrid pultruded composites for structural applications, Materials, 17(2), 302. DOI: 10.3390/ma17020302.
[22] Zaghloul, M. Y., Zaghloul, M. M. Y., Zaghloul, M. M. Y. (2022). Influence of stress level and fibre volume fraction on fatigue performance of glass fibre-reinforced polyester composites, Polymers, 14(13), 2662. DOI: 10.3390/polym14132662.
[23] Alajarmeh, O., Malano, A., Ferdous, W., Almasabha, G., Tarawneh, A., Awward, K. E., Safonov, A., Zeng, X., Schubel, P. (2023). Fatigue behavior of unidirectional fiber-reinforced pultruded composites with high volume fiber fraction, Fatigue Fract. Eng. Mater. Struct., 46(6), pp. 2034–2048. DOI: 10.1111/ffe.13979.
[24] Fatemi, A., Yang, L. (1998). Cumulative fatigue damage and life prediction theories: a survey of the state of the art for homogeneous materials, Int. J. Fatigue., 20(1), pp. 9–34. DOI: 10.1016/S0142-1123(97)00081-9.
[25] Degrieck, J., Van Paepegem, W. (2001). Fatigue damage modeling of fibre-reinforced composite materials, Appl. Mech. Rev., 54(4), pp. 279–300. DOI: 10.1115/1.1381395.
[26] Post, N. L., Case, S. W., Lesko, J. J. (2008). Modeling the variable amplitude fatigue of composite materials: A review and evaluation of the state of the art for spectrum loading, Int. J. Fatigue., 30(12), pp. 2064–2086. DOI: 10.1016/j.ijfatigue.2008.07.002.
[27] Sevenois, R. D. B., Van Paepegem, W. (2015). Fatigue damage modeling techniques for textile composites: review and comparison with unidirectional composite modeling techniques, Appl. Mech. Rev., 67(2), 020802. DOI: 10.1115/1.4029691.
[28] Khan, A., Azad, M. M., Sohail, M., Kim, H. S. (2023). A review of physics-based models in prognostics and health management of laminated composite structures, Int. J. Precis. Eng. Manuf. - Green Technol., 10, pp. 1615–1635. DOI: 10.1007/s40684-023-00509-4.
[29] Bogdanov, A. A., Panin, S. V., Kosmachev, P. V. (2023). Fatigue damage assessment and lifetime prediction of short fiber reinforced polymer composites – A review, J. Compos. Sci., 7, 484. DOI: 10.3390/jcs7120484.
[30] Yang, J. N., Jones, D. L., Yang, S. H., Meskini, A. (1990). A stiffness degradation model for graphite/epoxy laminates, J. Compos. Mater., 24(7), pp. 753–769. DOI: 10.1177/002199839002400705.
[31] Whitworth, H. A. (1998). A stiffness degradation model for composite laminates under fatigue loading, Compos. Struct., 40(2), pp. 95–101. DOI: 10.1016/S0263-8223(97)00142-6.
[32] Mao, H., Mahadevan, S. (2002). Fatigue damage modelling of composite materials, Compos. Struct., 58(4), pp. 405–410. DOI: 10.1016/S0263-8223(02)00126-5.
[33] Van Paepegem, W., Degrieck, J. (2002). A new coupled approach of residual stiffness and strength for fatigue of fibre-reinforced composites, Int. J. Fatigue, 24(7), pp. 747–762. DOI:10.1016/S0142-1123(01)00194-3.
[34] Wu, F., Yao, W. X. (2010). A fatigue damage model of composite materials, Int. J. Fatigue, 32(1), pp. 134–138. DOI: 10.1016/j.ijfatigue.2009.02.027.
[35] Shiri, S., Yazdani, M., Pourgol-Mohammad, M. (2015). A fatigue damage accumulation model based on stiffness degradation of composite materials, Mater. Des., 88, pp. 1290–1295. DOI: 10.1016/j.matdes.2015.09.114.
[36] Zong, J., Yao, W. (2017). Fatigue life prediction of composite structures based on online stiffness monitoring, J. Reinf. Plast. Compos., 36(14), pp. 1038–1057. DOI: 10.1177/0731684417701198.
[37] Wang, C., Zhang, J. (2020). Experimental and analytical study on residual stiffness/strength of CFRP tendons under cyclic loading, Materials, 13(24), 5653. DOI: 10.3390/ma13245653.
[38] Gao, J., Yuan, Y. (2020). Probabilistic modeling of stiffness degradation for fiber reinforced polymer under fatigue loading, Eng. Fail. Anal., 116, 104733. DOI: 10.1016/j.engfailanal.2020.104733.
[39] Gao, J., Zhu, P., Yuan, Y., Wu, Z., Xu, R. (2022). Strength and stiffness degradation modeling and fatigue life prediction of composite materials based on a unified fatigue damage model, Eng. Fail. Anal., 137, 106290. DOI: 10.1016/j.engfailanal.2022.106290.
[40] Gao, J.-X., Heng, F., Yuan, Y.-P., Liu, Y.-Y. (2023). Fatigue reliability analysis of composite material considering the growth of effective stress and critical stiffness, Aerospace, 10(9), 785. DOI: 10.3390/aerospace10090785.

[41] Staroverov, O. A., Mugatarov, A. I., Yankin, A. S., Wildemann, V. E. (2023). Description of fatigue sensitivity curves and transition to critical states of polymer composites by cumulative distribution functions, Frattura ed Integrità Strutturale, 17(63), pp. 91–99. DOI: 10.3221/IGF-ESIS.63.09.
[42] Wildemann, V., Staroverov, O., Strungar, E., Mugatarov, A., Kuchukov, A. (2023). Mechanical properties degradation of fiberglass tubes during biaxial proportional cyclic loading, Polymers, 15(9), 2017. DOI: 10.3390/polym15092017.
[43] Wildemann, V. E., Staroverov, O. A., Mugatarov, A. I., Kuchukov, A. M. (2023). Fatigue sensitivity of GFRP under proportional cyclic tension with torsion, PNRPU Mechanics Bulletin, 6, pp. 29–40. DOI: 10.15593/perm.mech/2023.6.03.
[44] Basquin, O.H. (1910). The exponential law of endurance tests, ASTM Proc., 10, pp. 625–630.
[45] Wildemann, V., Strungar, E., Lobanov, D., Mugatarov, A., Chebotareva, E. (2023). Experimental study of postcritical deformation stage realization in layered composites during tension using digital image correlation and acoustic emission, Acta Mechanica Sinica. DOI: 10.1007/s10409-023-23468-x. Available at: https://www.sciengine.com/AMS/doi/10.1007/s10409-023-23468-x
[46] Wildemann, V, Staroverov, O, Strungar, E, Lunegova, E, Mugatarov, A. (2022). Stability of postcritical deformation of CFRP under static ±45° tension with vibrations, Polymers, 14(21), 4502. DOI: 10.3390/polym14214502.
[47] Uppin, V. S., Gouda, P. S. S., Sridhar, I. (2023). Mechanisms for introduction of pseudo ductility in fiber reinforced polymer composites - A review, Frattura ed Integrità Strutturale, 65, pp. 17–31. DOI: 10.3221/IGF-ESIS.65.02.
[48] Gudadappanavar, B., Kulkarni, D., Gouda, S. (2023). An assessment of HDPE fillers and fiber wrapping on the strength of reinforced concrete, Frattura ed Integrità Strutturale, 64, pp. 240–249. DOI: 10.3221/IGF-ESIS.64.16.